Trajectory Analysis of Summertime Sulfate Concentrations in the Northeastern United States

PERRY J. SAMSON

Department of Atmospheric and Oceanic Science, The University of Michigan, Ann Arbor 48109

(Manuscript received 11 November 1979, in final form 7 July 1980)

ABSTRACT

This paper presents a technique for quantifying the relationships between observed concentrations of atmospheric sulfate aerosol and their corresponding upstream history of sulfur dioxide emissions, wind speed and mixing height. Using reported sulfate concentrations from several sampling sites in the northeastern United States, 72 h upstream trajectories have been computed for winds in the mixed layer of the atmosphere over the duration of their respective sampling periods.

Trajectories from one site were computed for four sublayers, each 400 m thick, extending from the surface to 1600 m. The deviations in along-trajectory and cross-trajectory directions of each of the sublayers from the position of the whole mixed layer were computed. From this the functions $\sigma_y(t)$ and $\sigma_x(t)$ for travel times of 6 to 72 h were derived for each layer individually and collectively for the whole layer. The values of $\sigma_y(t)$ and $\sigma_x(t)$ for the whole mixed-layer were found to be roughly equivalent over this time period and to grow linearly in time. The growth can be described by the relationship $\sigma_y(t) = 5.4t$, where σ_y is in kilometers and t is in hours.

Using these statistics to describe the potential impact from upstream sources, each trajectory was integrated over finite time steps to estimate the potential emissions loading along that trajectory as a function of time upstream. Correspondingly, estimates were made as a function of time upstream of the wind speed in the layer and the depth of the mixed layer.

It was found that sulfate concentrations were insensitive to upstream mixing height, as determined in this study, but were almost always positively correlated with the inverse of wind speed occurring 24 h or more upstream of the sampling point. No consistent relationship was evident between sulfate concentrations and potential upstream SO_2 emissions loading.

The ratio of observed to potential sulfate generation, as determined from the total upstream sulfur dioxide input, indicates an average net efficiency of roughly 15–30% conversion of sulfate dioxide to sulfate before deposition. These values vary dramatically with increasing efficiency corresponding to increasing resultant sulfate concentration.

1. Introduction

The investigation of atmospheric aerosols containing the sulfate ion $SO_4^=$ has recently become a focal point for environmental and energy-related research programs. In the United States the level of demand for energy, coupled with economic and political pressures on other sources of energy, are requiring the use of domestic coal on an ever increasing scale. Unfortunately, much of the readily available coal contains a small percentage of sulfur which, upon combustion, produces gaseous sulfur oxides. These emissions can then undergo chemical transformation in the atmosphere to produce sulfate aerosols.

The growth of interest in atmospheric sulfates has been spurred on by investigations in at least three important areas of environmental concern. First, sulfate has been linked in epidemiological and laboratory studies with possible adverse effects on human health (Amdur *et al.*, 1972; EPA, 1974; McJilton *et al.*, 1973). Second, dissolved sulfate has also often been cited as a primary contributor to the acidification of precipitation (Granat, 1972; Likens, 1976; Galloway *et al.*, 1976). Finally, sulfates are thought to be a major contributor to the reduction in visibility caused by atmospheric aerosols (Waggoner *et al.*, 1975) because the characteristic size range of the aerosol is within 0.1–1.0 μm (Whitby, 1978) which is efficient in scattering light.

Much has already been learned about the nature of the sulfate aerosol. It has been shown by Hall *et al.* (1975), Samson and Ragland (1977) and Wolff *et al.* (1977) that large areas of very low visibility, believed to be a surrogate for the sulfate aerosol, can cover several thousands of square kilometers during the summer months. These areas can exist for several days and can be tracked as they are advected by the boundary-layer flow.

It has also been theorized that the sulfate aerosol can be transported over long distances and could

0021-8952/80/121382-13$07.25

pose problems for rural areas otherwise unaffected by human pollution. Stasiuk *et al.* (1975) noted relatively high concentrations of sulfate at the summit of Whiteface Mountain in the Adirondacks of New York State. Subsequently, Lioy *et al.* (1977) and Galvin *et al.* (1978) have indicated that high concentrations of sulfate measured in rural upstate New York can probably be attributed to emissions of SO_2 occurring many kilometers upwind in areas of high sulfur emissions. Chung (1978) has shown similar evidence for sulfate transport into Ontario, Canada.

Much of our present knowledge about the formation, movement and eventual decay of region-scale episodes of high sulfate concentrations has been obtained from spatial and temporal examination of individual periods. However, there is a need to evaluate observed concentrations of sulfate in a more climatological sense. This paper presents a methodology for objectively diagnosing upstream factors which could have influenced the observed sulfate concentrations. The estimated upstream SO_2 emissions loading, wind speed and mixing depth are then correlated with observed concentrations of sulfate in the northeastern United States.

2. Trajectory analysis

a. Trajectory model

The trajectory model of Heffter *et al.* (1975), modified to compute the trajectory of an air column within the mixed layer of the atmosphere, is used in this study. Observed upper air temperature profiles are scanned through the first 2500 m to locate the top of the mixed-layer, which is defined as the base of the first non-surface-based inversion. If no inversion is found, the model assumes a preselected default value. The model then scans the observed wind profiles and determines the base of the mixed-layer to be the height at which the shear of the wind velocity becomes <5 m s^{-1} between adjacent observation heights. If such a shear zone is missing, the model integrates upward from the surface. If the layer of shear exceeds 500 m, the model integrates from 500 m to the top of the layer. An average wind velocity is computed for the layer at each station and the models interpolates between stations to compute the trajectories.

Trajectories locations are computed at three hour intervals using the observed winds within a 480 n mi radius of the trajectory location. Winds are weighted according to the inverse of distance squared and also downwind direction ψ as $(1 - 0.5|\sin\psi|)$. Trajectories are computed using station data where at least two reporting levels are available for averaging in the specified layer and only for those segments where at least two reporting stations are within the 480 km limit or one station is within 240 km.

b. Potential contribution functions

The use of a mixed-layer trajectory model assumes that the material being traced is moving with the mean motion of the mixed layer. This assumption will only be true if the material is, in fact, well-mixed through the layer and if there is no shear in the layer to disperse the material away from the mean flow.

In order to estimate the potential upstream emissions loading which could contribute to the degradation of air quality in the volume of air sampled it is necessary to statistically define the upstream probability distribution functions or potential contribution functions which describe the probability of a particular source impacting upon a given receptor given a particular trajectory path. To determine this function for general summertime conditions upstream trajectories were computed for four preset layers of the atmosphere, each 400 m thick, extending from the surface to 1600 m. Trajectories were also computed separately for the whole sfc–1600 m layer. These were computed each 12 h for a period of 66 days from 13 June to 17 August 1977, corresponding to the period of sulfate collection of the 1977 New York State Sulfate Network (Coffey *et al.*, 1979). The trajectories were computed 72 h upstream from a sampling point in rural western New York (Holland, New York; 42.64°, 78.53°).

A discussion of the dispersion within a layer of the atmosphere requires the consideration of both 1) the perturbations over time at each level within the layer from the mean motion of that level and 2) the divergence of the mean motions of each level from the mean motion of the whole layer. Consider a coordinate axis following the mean motion of the mixed-layer. At each height z within the layer, a probability distribution function can be tabulated from a sample population of trajectories by considering their lateral perturbations y' from the location of the whole mixed-layer trajectory as a function of time t upstream. Each level will have its own mean displacement, $\bar{y}(z;t)$, from the location of the mixed-layer trajectory about which its perturbations will be distributed. Let the perturbations about $\bar{y}(z,t)$ be described by a probability distribution function $f(y,z;t)$. The concentration pattern observed at the surface will be the net result of transport and dispersion occurring through all (or parts) of the whole mixed layer, depending on the lateral and vertical distribution of pollutant $\omega(y,z;t)$. If $g(y;t)$ is the probability distribution function describing the potential contribution of sources adjacent to the location of the mixed-layer trajectory at time t to the resultant air quality at the terminal

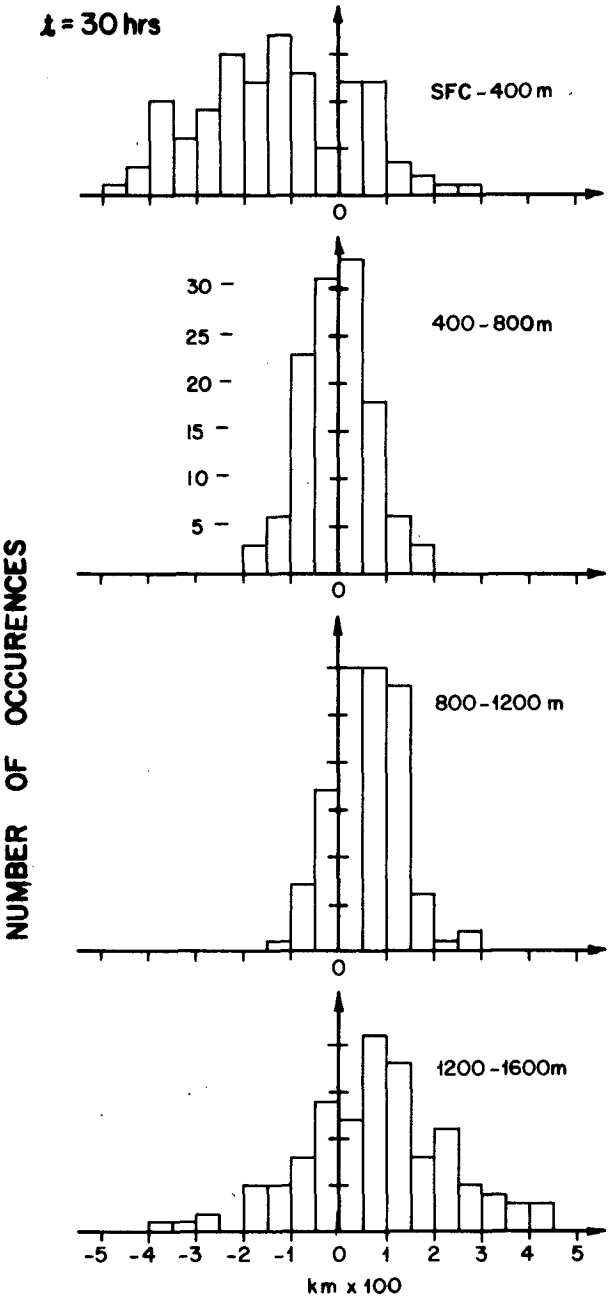

FIG. 1. Frequency distributions of cross-trajectory perturbations from the mean flow for the whole 1600 m layer at 30 h upstream for each of the 400 m sublayers.

point, it can be expressed as

$$g(y,t) = \int_{h_0}^{h_1} f(y,z,t)\omega(y,z,t)dz, \qquad (1)$$

where h_0 and h_1 are the bottom and top of the layer of interest.

Evaluation of the terms in Eq. (1) is limited due to the non-continuous nature of available wind data in the vertical. So, rather than consider continuous individual levels we consider discrete sublayers l of the whole layer. In this study the probability distribution functions of lateral perturbations in four layers are determined independently and the probability distribution function of source impact for the whole layer is computed using a discrete form of Eq. (1) as

$$g(y,t) = \sum_{l=1}^{4} f_l(y,t)\omega_l, \qquad (2)$$

where $f_l(y;t)$ is the probability distribution function in y at t hours upstream for sublayer l. The proportionality factor, ω_l, describes the vertical distribution of pollutant concentrations, assumed constant in time and space, over the four sublayers such that $\sum \omega_l$, summed from $l = 1$ to $l = 4$, equals 1.

If the distributions in each sublayer are normal probability distributions with a mean lateral displacement $\bar{y}_l(t)$ from the whole-layer location and standard deviation $\sigma_y(t)_l$, Eq. (2) can be rewritten by substituting the normal probability distribution function for each of the four sublayers to be

$$g(y,t) = \sum_{l=1}^{4} \frac{\omega_l}{\sqrt{2\pi}[\sigma_y(t)]_l} \exp\left\{\frac{-y_l'^2}{2[\sigma_y(t)]_l^2}\right\}, \qquad (3)$$

where y_l' is the lateral displacement from $\bar{y}_l(t)$.

An approach similar to one employed by Durst (1959) and later Bolin and Persson (1975) for obtaining standard vector deviations from climatological trajectory calculations has been modified for use in this analysis. At each segment endpoint the along-trajectory and cross-trajectory deviations from the locations of the whole-layer trajectory were computed for each of the four sublayers.

Trajectory calculations were terminated if their path traveled out of the range of available data (over the oceans or north of 55° latitude). Thus, out of the possible sample size of 134 trajectory groups (66 days × 2 day^{-1}), the available sample size ranged from 134 at $t = 3$ h upstream to 62 at $t = 72$ h upstream.

Fig. 1 shows the distribution functions of the lateral perturbations for each of the four sublayers studied at $t = 30$ hours upstream. The perturbations from the mean motion of the whole 1600 m layer for the sublayer from the surface to 400 m are centered toward the left of the mean motion looking upstream. The two layers, 400–800 m and 800–1200 m, are more aligned with the mean motion of the whole layer and have a smaller spread of values than did the first 400 m layer. The highest 400 m layer considered has a relatively large range of values and are centered toward the right of the mean motion.

The individual probability distribution functions in Fig. 1 can be shown to approximate normality to a reasonable degree of probability. Goodness of fit analysis using the χ^2 test between these distribu-

TABLE 1. The standard deviations of cross-trajectory perturbations for four layers of 400 m depth from the surface to 1600 m as a function of travel time.

t (hr)	σ_y (km)			
	0–400 m	400–800 m	800–1200 m	1200–1600 m
6	20.5	9.9	11.1	19.4
12	37.7	15.6	20.1	35.1
18	56.1	23.3	29.1	52.2
24	78.7	29.2	43.0	74.8
30	99.9	34.6	54.3	93.6
36	125.2	39.1	58.4	107.5
42	151.1	43.7	70.1	136.1
48	170.1	47.0	73.2	139.2
54	175.8	53.0	76.5	141.4
60	194.1	62.8	88.2	157.8
66	235.7	68.6	106.5	186.2
72	243.8	77.1	116.3	184.1

tions for *all* upstream times and the frequency of the occurrence expected by the normal distribution were conducted. It was found that at the 5% level of significance the distributions in all cases considered were consistent with the hypothesis that the observed distributions were normal.

A summary of the computed standard deviations in the cross-trajectory direction for each of the four sublayers is listed in Table 1. The largest standard deviations occur in the lowest layer (sfc–400 m) with the smallest deviations in the next highest layer (400–800 m). The growth of σ_y with time is illustrated in Fig. 2 for each of the layers. Also, shown in the figure is the assumed growth of σ_y prescribed by Heffter *et al.* (1975), $\sigma_y = 1.8\ t$, where σ_y is in kilometers and t is in hours. The basic slope of these derived functions do not appear to differ significantly from the linear relationship estimated by Heffter.

While standard deviation in the along-trajectory direction can be ignored for studies of continuous plumes, this study integrates over discrete upstream segments of the trajectories to ascertain the time-dependent emissions loading of SO_2. Thus, the corresponding σ_x values also have been computed and these are also shown in figure 2. Comparison of the two parameters indicates that σ_x has roughly the same slope and magnitude as σ_y.

The function $g(y;t)$ can be displayed graphically if the weighting function ω_l can be deduced or assumed. If we assume $\omega_1 = 1$ and $\omega_2 = \omega_3 = \omega_4$

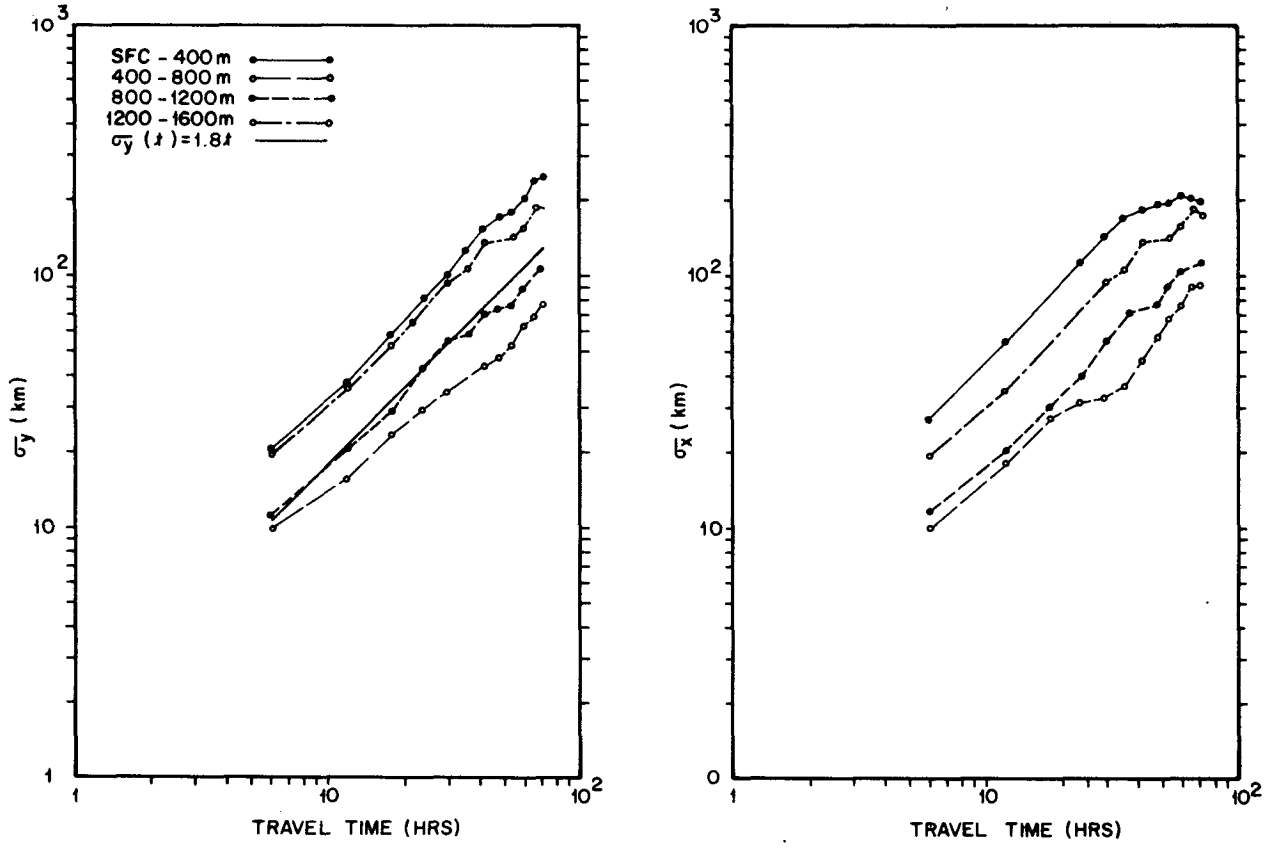

FIG. 2. The σ_y and σ_x values derived in this study as a function of travel time for each of the four sublayers for which trajectories were computed. Also shown is Heffter *et al.*'s (1975) empirical function $\sigma_y(t) = 1.8t$.

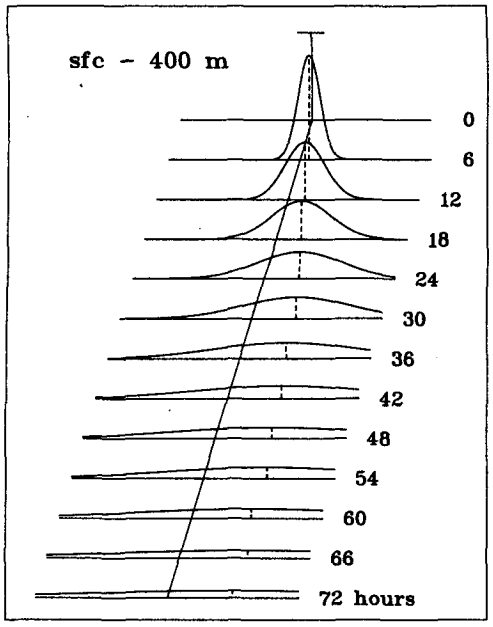

FIG. 3. The probability distribution function of cross-trajectory perturbations for the sfc–400 m sublayer. The location of the maximum probability at each time interval upstream is denoted by a dashed line. The scale at $t = 0\,h$ is equivalent to 0.01 km^{-1}. The width shown at each time interval is ±400 km.

$= 0$, then the resulting probability distribution function describes the potential of contribution to the resultant air quality resulting from transport in the sfc–400 m layer relative to the location of the whole-layer trajectory. The potential contribution function for the layer from the surface to 400 m is shown in Fig. 3. The center line of maximum probability for this layer originates from the right of the motion of the whole layer looking downstream.

Similarly by sequentially setting ω_l equal to unity the potential contribution functions for each of the other three sublayers can be calculated. The next two layers (400–800 m and 800–1200 m) have much sharper distributions than the lowest layer and tend to follow the center line of the mean motion of the whole layer more closely. The distribution of the perturbations in the 1200–1600 m layer has a larger scatter than the middle two layers. This may be due to the fact that this layer periodically transects the top of the mixed layer and hence is influenced by wind shears existing across that boundary.

If it is assumed that the whole layer is well mixed and that the sublayers all contribute equally to the transport of material to the site, i.e., $\omega_1 = \omega_2 = \omega_3 = \omega_4 = 0.25$, then the potential contribution function for the whole layer calculated using Eq. (3). Table 2 lists the values of $\sigma_y(t)$ and $\sigma_x(t)$ for perturbations of the four layers combined. These values are larger than those found for the individual sublayers since the divergence of the mean sublayer displacements (climatological vertical shear) contributes significantly to the dispersion. When plotted versus travel time (Fig. 4) the $\sigma_y(t)$ values have a similar slope but a much larger magnitude than the values of Heffter *et al.*'s approximation.

In fact, linear regression of the sigma values indicates that a simple linear relationship of the form

$$\sigma_y(t) \approx \sigma_x(t) = 5.4t, \qquad (4)$$

where σ_y is in kilometers and t in hours, explained over 90% of the variance of the sigma values. Hence, sigma values three times those recommended by Heffter *et al.* (1975) have been used in this study for describing horizontal dispersion over long travel times in the mixed layer of the atmosphere.

The spatial distribution of the potential contribution field for a hypothetical trajectory arriving at Holland, New York, is shown in Fig. 5. This represents the assumption that all layers between the surface and 1600 m contributed equally to the observed concentration at Holland. It is clear that the probability field expands substantially upstream of the sampling point. Thus the confidence of identifying the individual source regions contributing to an observed concentration would be expected, in general, to be small at 36 or more hours upstream.

3. Ensemble analysis

a. Mean layer wind speed

The calculation of the wind speed along the trajectory is accomplished by computation of the net distances between successive 3 h upstream segment endpoints, divided by the time step. The net distance between trajectory segment endpoint j and the preceding endpoint is calculated as

$$\Delta x_j = R[(\Delta\lambda_j^2)\cos^2\phi_j + (\Delta\phi_j^2)]^{1/2}, \qquad (5)$$

where $\Delta\phi_j = \phi_j - \phi_{j-1}$ and $\Delta\lambda_j = \lambda_j - \lambda_{j-1}$ are the changes in latitude and longitude, respectively, and R is the ratio of kilometers to degrees latitude.

TABLE 2. The standard deviations of along- and cross-trajectory displacements of the ensemble of four sublayers from the surface to 1600 m as a function of travel time.

t(h)	σ_x(km)	σ_y(km)	t(h)	σ_x(km)	σ_y(km)
3	23.2	20.9	39	250.6	197.4
6	41.5	33.2	42	246.8	224.5
9	61.8	44.8	45	256.4	224.0
12	80.0	60.0	48	265.3	241.2
15	102.8	72.5	51	279.2	247.2
18	119.2	88.8	54	292.3	249.7
21	140.0	100.4	57	314.3	255.1
24	154.2	125.3	60	309.3	276.6
27	177.9	140.3	63	324.8	297.0
30	193.9	157.4	66	314.1	330.2
33	210.7	169.9	69	333.4	332.5
36	228.5	184.5	72	312.3	339.6

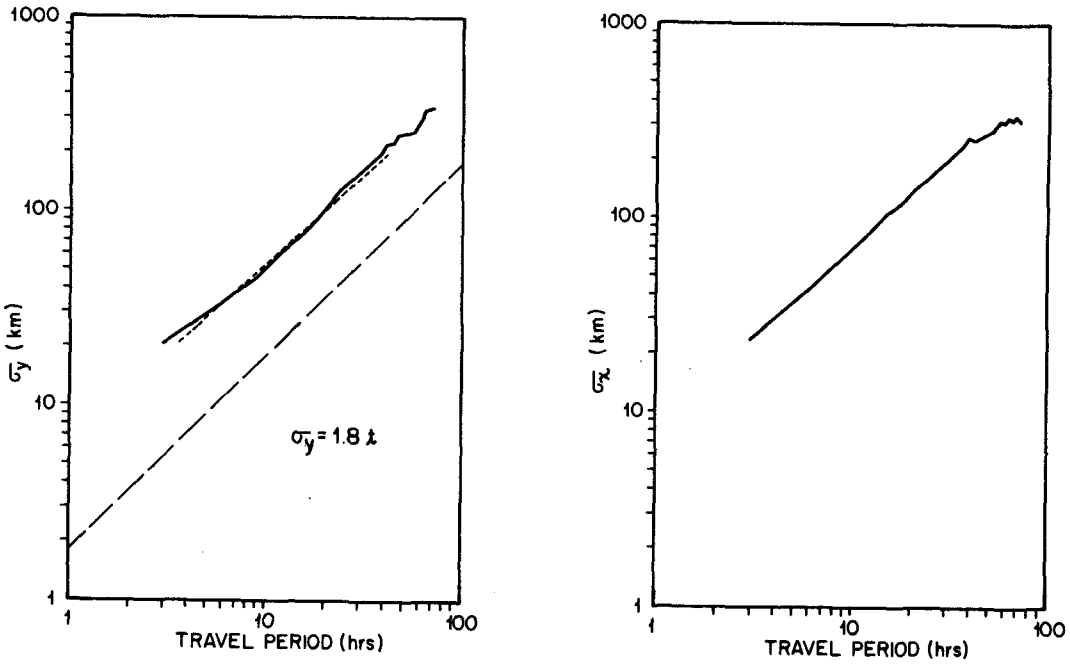

FIG. 4. The σ_y and σ_x values derived in this study for the whole layer, sfc–1600 m. Also shown is Heffter *et al.*'s (1975) empirical function $\sigma_y(t) = 1.8t$.

b. Mean mixing depth

The mixed-layer depth was computed using the methodology of the ARL trajectory model as described earlier. These values are interpolated to the trajectory location using the same interpolation scheme as that used for wind velocity.

Unfortunately, this methodology is quite stringent

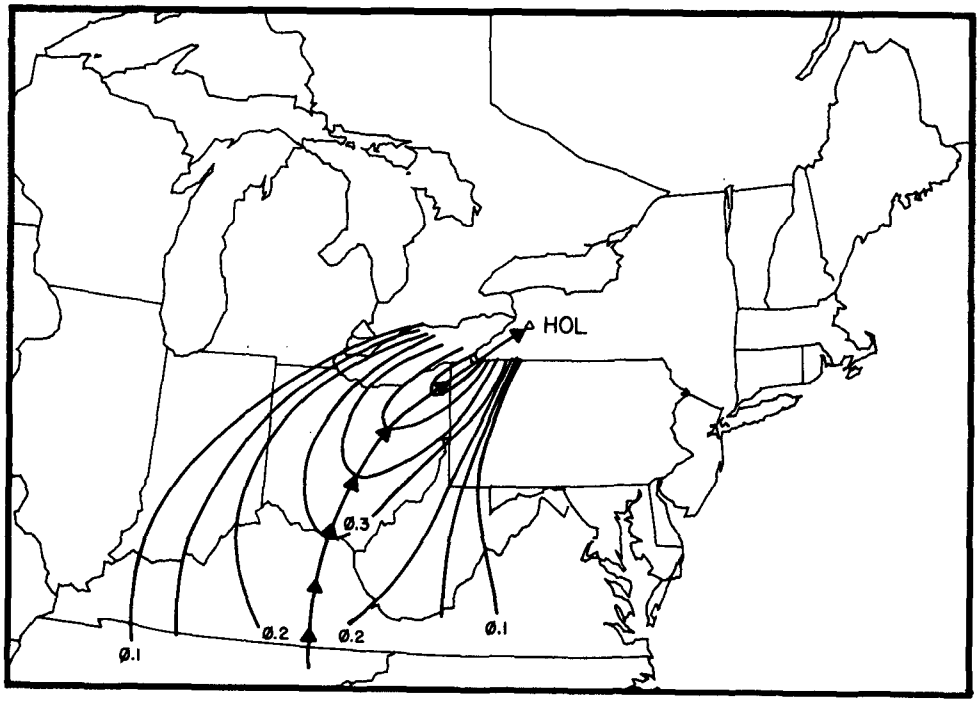

FIG. 5. A hypothetical mixed-layer trajectory arriving at Holland, New York, showing the integrated potential contribution field if it is assumed that all sublayers contribute equally to the observed concentrations. Units are $km^{-1} \times 100$ lateral from the location of the mixed-layer trajectory. The arrowheads represent travel increments of 6 h duration.

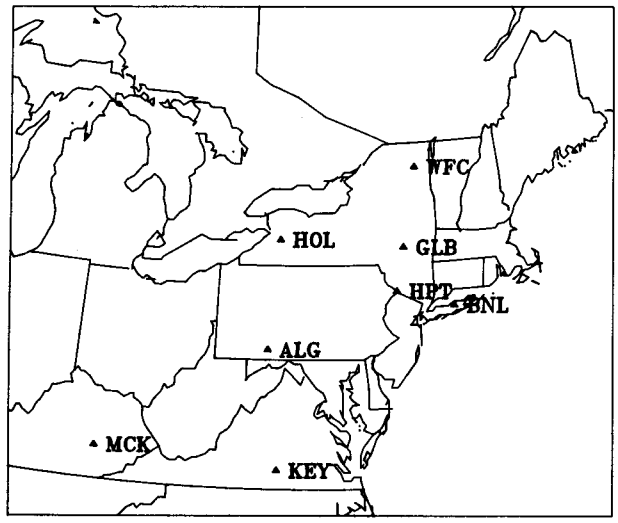

FIG. 6. Locations of the sulfate sampling locations used in this study. A listing of the station names, along with the dates of operation and the investigator(s) responsible appears in Table 3.

and does not find an elevated inversion in many cases.[1] When no inversion is found the model assumes a default value (1500 m was chosen as the default value here) as the top of the mixed layer for that site.

c. Emissions burden

The emissions grid used in this study was derived from the Brookhaven National Laboratory data base of summertime point source emissions east of the Mississippi River. These data merge emissions inventories obtained from the EPA National Emissions Data system and the Federal Power Commission. An emissions inventory for the Province of Ontario, Canada, was obtained from the Ontario Ministry of the Environment. While absolute emissions may vary substantially in time from source to source, this study is concerned with the spatial deployment of emissions. Over a substantially long study period such oscillations would be expected to be unimportant.

The point source emissions data was tabulated onto a grid of 0.50° longitude by 0.38° latitude (so that the sides of the grid cells were equal at 40°N). The summed total emissions within a grid cell were divided by the area, which ranged from roughly 1500 km^2 at 50°N to 2100 km^2 at 28°N, to arrive at an estimate of the emissions strength over the cell in units of kg km^{-2} h^{-1}.

If we define that field as $Q_{m,n}$ with $m = 1, M$ columns and $n = 1, N$ rows, it is possible to integrate over finite segments of trajectory to estimate the emissions loading. The integration is performed by dividing the trajectory segment of interest into twelve equal increments of length $\delta x = \Delta x/12$. The length Δx is the distance covered by the air column in the time interval from t hours upstream to $t + \Delta t$ hours upstream. The mean width of the emissions cell normal to the trajectory segment is denoted by δy. Then the integration over the segment can be approximated by

$$q = \frac{1}{2\pi} \sum_{n=1}^{N} \sum_{m=1}^{M} \left\{ \sum_{k=1}^{12} \frac{Q_{m,n}\delta x \delta y}{\sigma_x(t)\sigma_y(t)} \times \exp\left[-\frac{1}{2}\left(\frac{x'^2}{\sigma_x^2(t)} + \frac{y'^2}{\sigma_y^2(t)} \right) \right] \right\}, \quad (6)$$

where q is the emissions integrated over the segment in units of kg km^{-1} h^{-1}, x' and y' are the along and cross-trajectory distances, respectively, from the trajectory at time t to grid location m,n.

4. Results

Fig. 6 shows the location of the sulfate sampling sites used in this study. A listing of the station names, along with dates of operation and investigators responsible appears in Table 3. All sites represent rural areas with negligible local emissions of sulfur dioxide. The reader is referred to the investigator's report for explanation of the chemical analyses employed and for descriptions of the sampling locations.

CATEGORIZATION OF TRAJECTORIES

The catagorization of trajectories into those corresponding to low resultant sulfate concentrations (<5 μg m^{-3}) and high resultants sulfate concentrations (>15 μg m^{-3}) gives a graphical description of the general "preferred" paths for the two conditions. Fig. 7–10 show the trajectories arriving closest to the middle of the individual sampling periods at Holland, New York, Allegheny Mountain, Pennsylvania, Keysville, Virginia, and McKee, Kentucky, respectively. The duration of travel between arrowheads is 6 h with each trajectory computed 72 h upstream (or until wind data was insufficient to continue).

The dichotomy between the high and low concentrations samples is striking at these stations. In Fig. 7 Holland received its lowest concentrations from the west to north, and were associated with relatively high winds in the layer of interest. The highest concentrations occurred with winds from the south to west with several observable cases of upwind stagnation (indicated by the looping pattern with shorter trajectory segments). The classification of Allegheny Mountain trajectories in Fig. 8 also shows a similar dichotomy.

[1] This methodology has subsequently been modified by Heffter (1980) to use potential temperature gradients for the estimation of mixed-layer depth.

TABLE 3. Sources of sulfate data along with investigator(s) and periods of study.

Site	Location	Investigators	Period
WFC	Whiteface Mtn., NY	Lioy et al. (1977)	1–31 July 1975
GLB	Gilboa, NY (Schoharie, NY)	Galvin et al. (1978)	6–31 July 1976
HOL	Holland, NY	Coffey et al. (1979)	15 June–15 Aug. 1977
HPT	High Point, NJ	Lioy et al. (1979)	1–15 Aug. 1977 (6 h)
BNL	Brookhaven Nat. Labs, NY	Tanner (1979)	18 July–30 Aug. 1977 (6 h)
KEY	Keysville, VA	Wolff et al. (1978)	19 June–21 July 1976 (4 h)
MCK	McKee, KY	Wolff et al. (1978)	3 Aug.–13 Sept. 1976 (4 h)
ALG	Allegheny Mtn., PA	Pierson et al. (1979)	26 July–11 Aug. 1977 (12 h)

The trajectories for Keysville, Virginia, in Fig. 9 follow a markedly different pattern. The lowest concentrations occur with a air flow from the south or with a few fast moving air trajectories from the northwest. The higher concentrations occur with slower moving air from the north and west and stagnant conditions to the southwest.

One of the most striking dichotomies occurs in the classification of trajectories for McKee, Kentucky, as shown in Fig. 10. Over the period of this study the lowest concentrations were associated with air flow from the north to northwest moving at moderately fast speeds despite passing over areas of relatively high emissions. The highest concentrations occur with a consistent pattern looping anticyclonically from the east. Since the trajectories to a point in Pennsylvania are similar to those shown in Fig. 8 for low concentrations at Allegheny Mountain, Pennsylvania, it would appear that chemical transformation south of that point must have been responsible for the high concentrations.

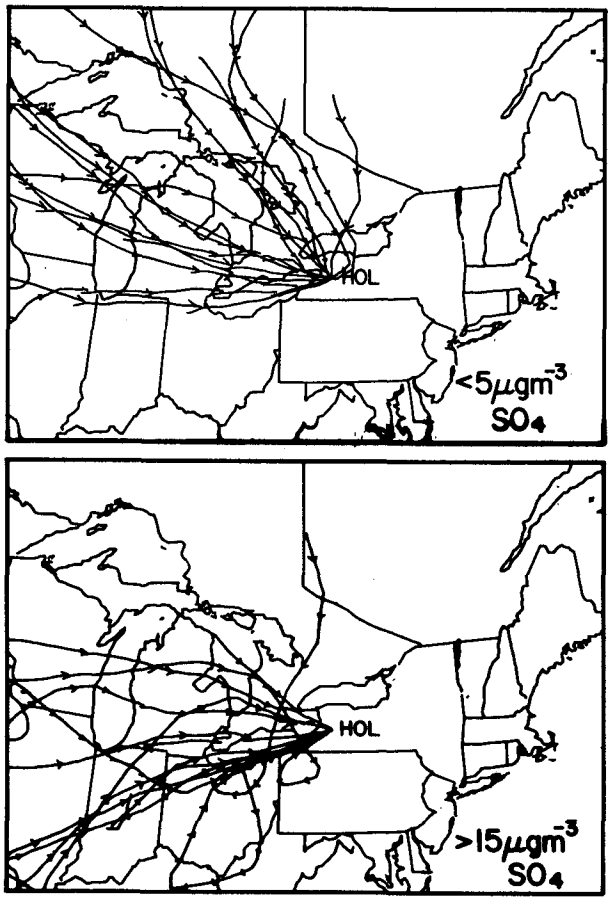

FIG. 7. Mixed-layer trajectories arriving at Holland, New York at 1400 EDT on days of low and high sulfate concentrations.

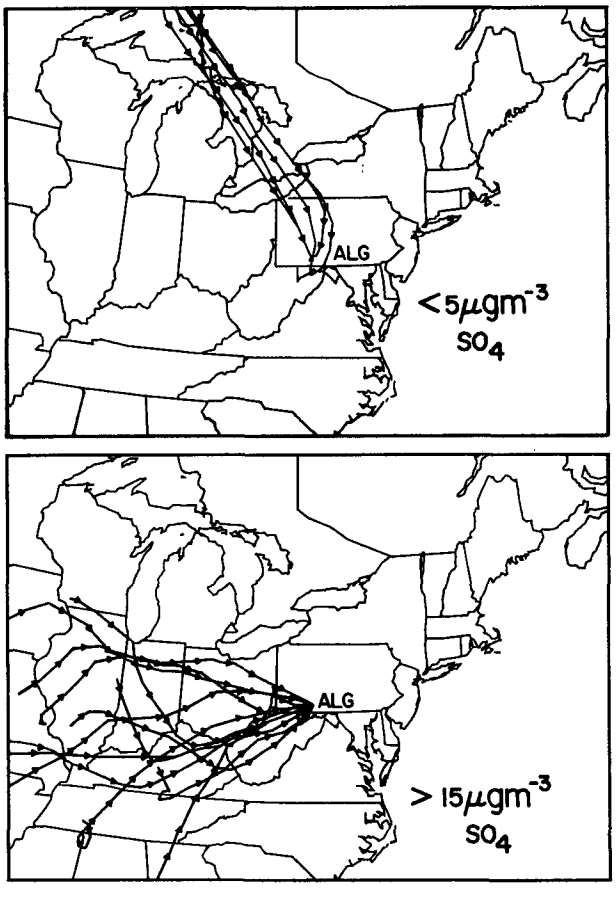

FIG. 8. Mixed-layer trajectories arriving at Allegheny Mountain, Pennsylvania at midpoint of 12 h sampling periods for low and high sulfate concentrations.

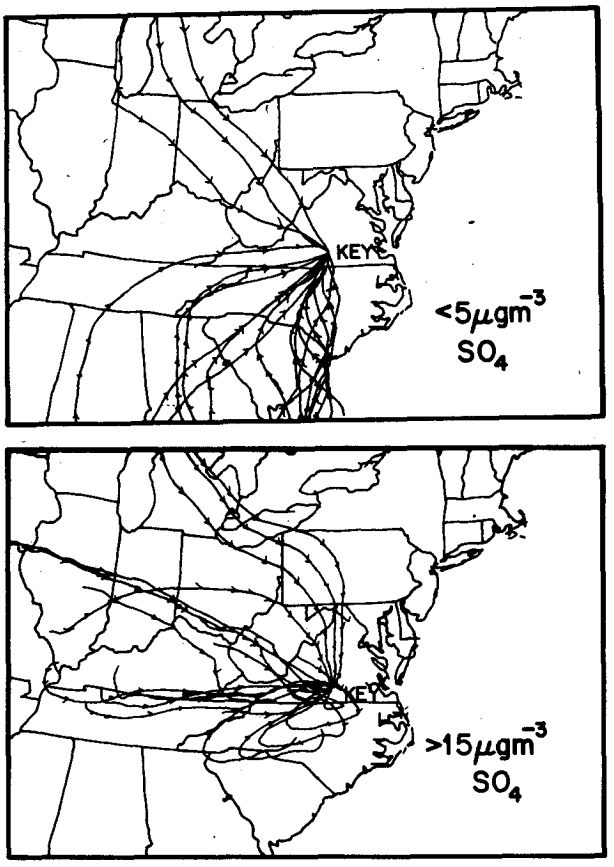

FIG. 9. Mixed-layer trajectories arriving at Keysville, Virginia, at midpoint of 4 h sampling periods corresponding to low and high sulfate concentrations.

5. Statistical relationships

a. Sulfate versus upstream mixing depth

Trajectories calculated for variable mixed layer depths from Holland, New York, over the period 15 June–15 August 1977 were used to compute the upstream mixing height h. Both the computed base and top of the mixed layer were stored.

In order to compare trajectory parameters with sulfate samples taken over periods >6 h (the time interval between trajectory calculations), it was necessary to average the trajectory parameters over the corresponding time period. For example, when 24 h samples were collected from midnight to midnight, an averaging of the form

$$\bar{h} = \tfrac{1}{4}[ph_0 + h_1 + h_2 + h_3 + (1 - p)h_4] \quad [7]$$

was used, where $\bar{h}$ is the average mixing height at a particular segment endpoint after averaging the estimated values: h_0, the estimated 0600 GMT mixing height; h_1, the 1200 GMT height, and so forth. The proportionality p depends on the relationship of the sampling period to the time zone lag from GMT.

The correlation coefficients for each upstream endpoint between the inverse of mixing height and the resultant sulfate concentration are shown in Fig. 12. For this set of data there is no apparent trend in the correlation pattern as a function of time upstream. The null hypothesis that the inverse of mixing height is not correlated to the resultant concentrations of sulfate cannot be rejected with confidence at any time upstream of the sampling location.

To check whether the depth of the morning surface inversion (the base of the mixed-layer) had any effect upon the resulting sulfate concentration downstream, linear regression was performed between those two variables as a function of hours upstream. Fig. 11 indicates that, at least for this set of data, no significant correlation was obtained.

These results should be viewed with some caution because, as was outlined earlier, the objective estimation of upstream mixing height requires further investigation before confidence can be placed on the results. Moreover, the deviations in mixing depth vary over a range of approximately ±50% during the summer while wind speed, the other component of atmospheric ventilation, varies over ±500%. Thus, the overall sensitivity of the resultant concentrations to changes in mixing height upstream

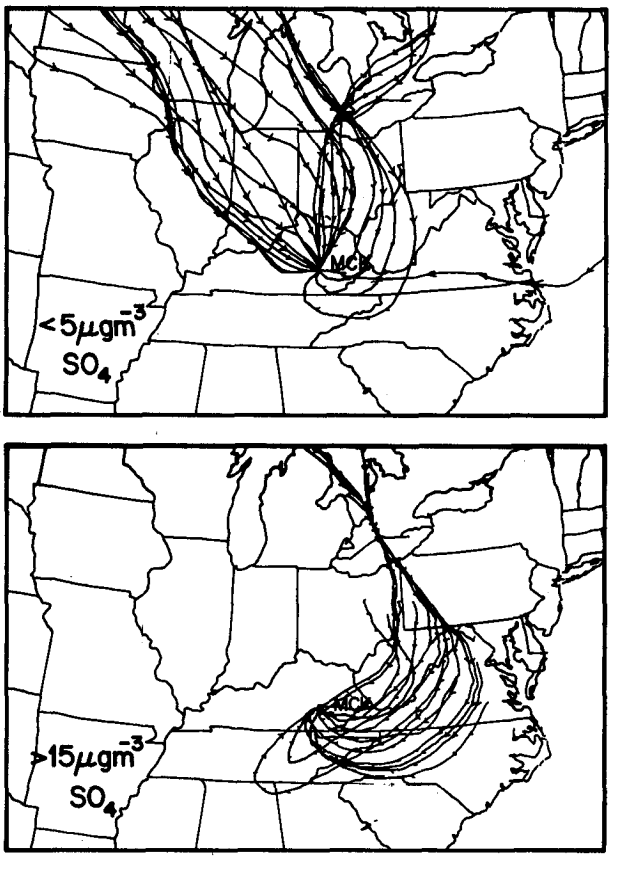

FIG. 10. As in Fig. 10 except for McKee, Kentucky.

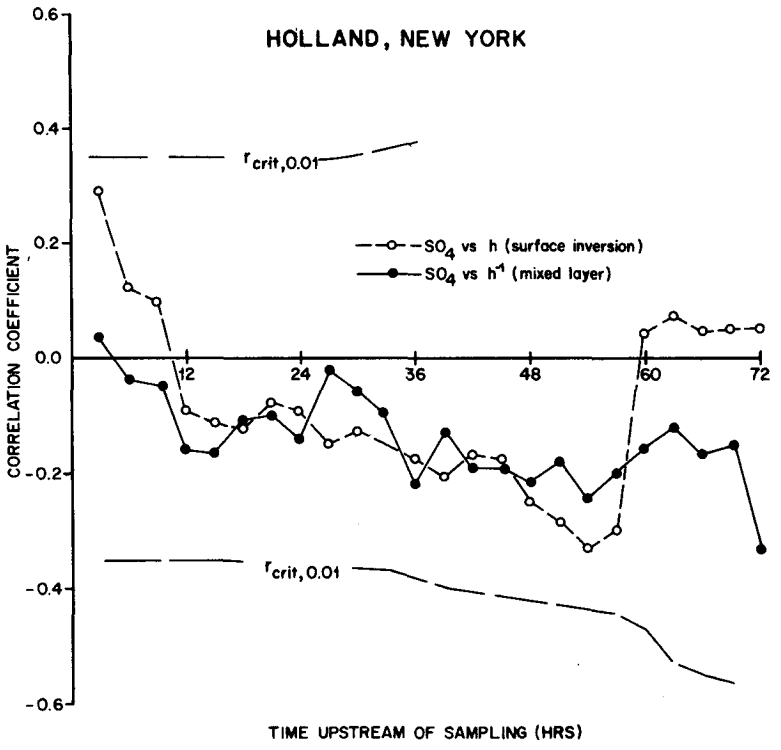

FIG. 11. Correlation coefficients as function of hours upstream between 1) the inverse of the mixed-layer depth and 2) the surface inversion depth and the resultant sulfate concentrations.

would be expected to be less than that for upstream wind speed.

b. SO_4 *versus upstream wind speed*

In an earlier paper (Samson, 1978) it was shown that the resultant concentration of sulfate measured at rural locations could be statistically explained, in part, by stagnation occurring more than 24 h upwind of the sampling point. Other sites, listed in Table 3, in the northeastern United States have been analyzed to see if similar trends exist.

Fig. 12 shows the correlation coefficients between the inverse of estimated wind speed and at each segment upstream and resultant sulfate and nitrate concentrations for High Point, New Jersey. The results are consistent with those reported previously by Samson (1978) for the upstate New York stations. For the period of this study, the changes in sulfate concentration could be statistically explained, in part, by stagnation occurring more than 48 h upstream. The nitrates, on the other hand, have a high correlation near the point of sampling. This result, though tentative because nitrate values were relatively low during the period and artifact nitrate production could have affected the results, would suggest local stagnation as being more important in the buildup of nitrate concentrations.

Fig. 13 shows these relationships for four other locations. In three of the four the previously discussed relationship appears to hold. Stagnation upstream of Keysville, Virginia, McKee, Kentucky, and Allegheny Mountain, Pennsylvania, was significantly correlated with resultant sulfate concentrations.

The exception occurred with the data collected at Brookhaven National Laboratory. The lack of correlation may be due to the mesoscale transport associated with the sea breeze, to which the trajectory model would be insensitive, or the variations in the sulfate may be in response to transport from the New York metropolitan region to its west, regardless of the far upstream conditions.

c. Sulfate versus upstream SO_2 *emissions*

The measured sulfate concentrations were also regressed with the upstream emissions loading of SO_2. To normalize the emissions per time segment the sulfate was correlated with q/U (kg km^{-2}).

Fig. 14 shows the correlation coefficients between these two variables for data collected at High Point, New Jersey. While there had been a significant correlation with the inverse of wind speed, no significant correlation can be discerned for emissions loading. In general, there is no consistent correlation pattern from station to station as

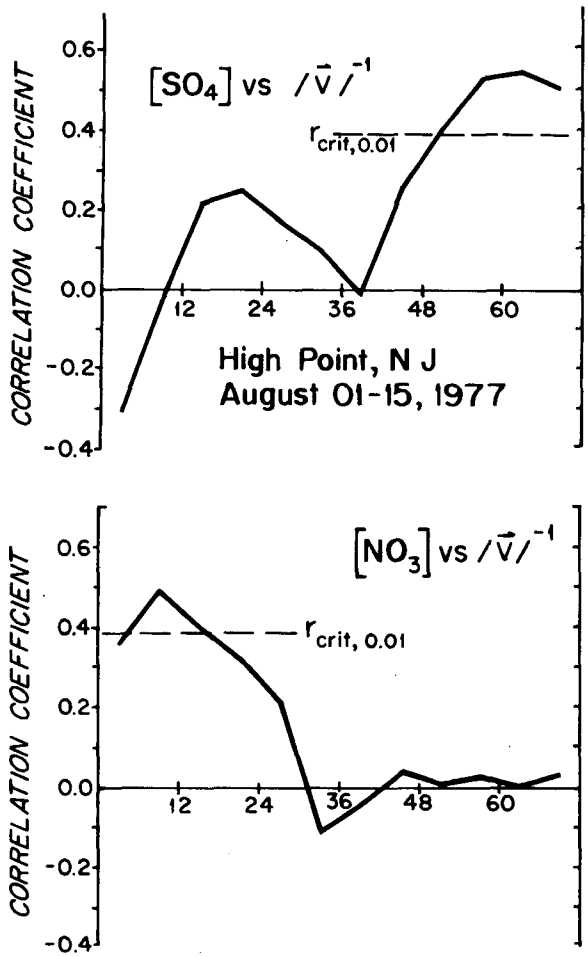

FIG. 12. Correlation coefficients as a function of hours upstream between the inverse of wind speed and resultant sulfate and nitrate concentrations for samples collected at High Point, New Jersey.

was evident from the correlation of sulfate with the inverse of wind speed alone.

A complete investigation of the budget of sulfur along the course of a trajectory would require Lagrangian measurements of the vertical profiles of sulfur dioxide and sulfate. Unfortunately, such data are not presently available. However, it is possible to make rough estimates of the net efficiency of the sulfur dioxide to sulfate conversion process for each trajectory.

By summing the emissions loading of SO_2 normalized by the ventilation over all the segments of the trajectory we can estimate the potential sulfate production along the route. If the efficiency ϵ is defined as the net change in SO_4 concentration over the whole trajectory divided by this potential production, then we can estimate the efficiency as

$$\epsilon = \frac{r_0 - r_J}{\frac{3}{2}\sum_{j=1}^{J} \frac{q_j}{U_j h_j}}, \qquad (8)$$

where r_0 is the observed SO_4 concentration at the terminus of the trajectory and r_J is the concentration J segments upstream. The concentration r_J is not usually known owing to the sparsity of data and has been set here to background level of 1.5 gm^{-3}. Thus these estimates are the upper limit on the efficiency of the conversion process since it is not uncommon for areas of high sulfate concentration to persist for several days.

The efficiency of each trajectory for each site was computed and these values were averaged over the sampling period to determine the average efficiencies. These values are tabulated in Table 4. The average efficiencies computed from this study imply that, as an upper limit, ~14–30% of the sulfur dioxide emitted into the atmosphere is being converted into sulfate aerosol before removal. This range is not inconsistent with the review of Rodhe (1978) who calculated, from estimates of turnover times, that ~30% of the sulfur dioxide is transformed to sulfate before being deposited.

As might be expected, the efficiency of the sulfur dioxide to sulfate system varies considerably from sample to sample. This variation is not random, however, because categorization of the efficiencies by resultant concentration produces a noticeable trend as shown in Table 5. In all cases the efficiencies decrease dramatically from the highest concentration classes to the lowest. This drop in estimated efficiency indicates poorer chemical conversion and/or more efficient removal for the lower concentration cases.

6. Conclusions

A new methodology for objectively estimating the upstream conditions which could influence sulfate concentrations has been developed. The description of the potential contribution functions based on the vertical shear of wind in the mixed layer allows upstream integration of SO_2 emissions to estimate the loading of anthropogenic sources to measured sulfate concentrations.

High concentrations of sulfates appear to be consistently associated with upstream stagnation. The magnitude of its correlation with stagnation, measured as the inverse of wind speed, is not improved by adding the magnitude of SO_2 emissions. Mixing height upstream was found to have no significant effect on resulting sulfate concentrations.

These results further emphasize the importance of meteorology in controlling the fluctuations in ambient sulfate measurements in the northeastern United States.

Acknowledgments. The sulfate data used in this study was generously provided by the following investigators: P. E. Coffey and P. J. Galvin, New York State Department of Environmental Conserva-

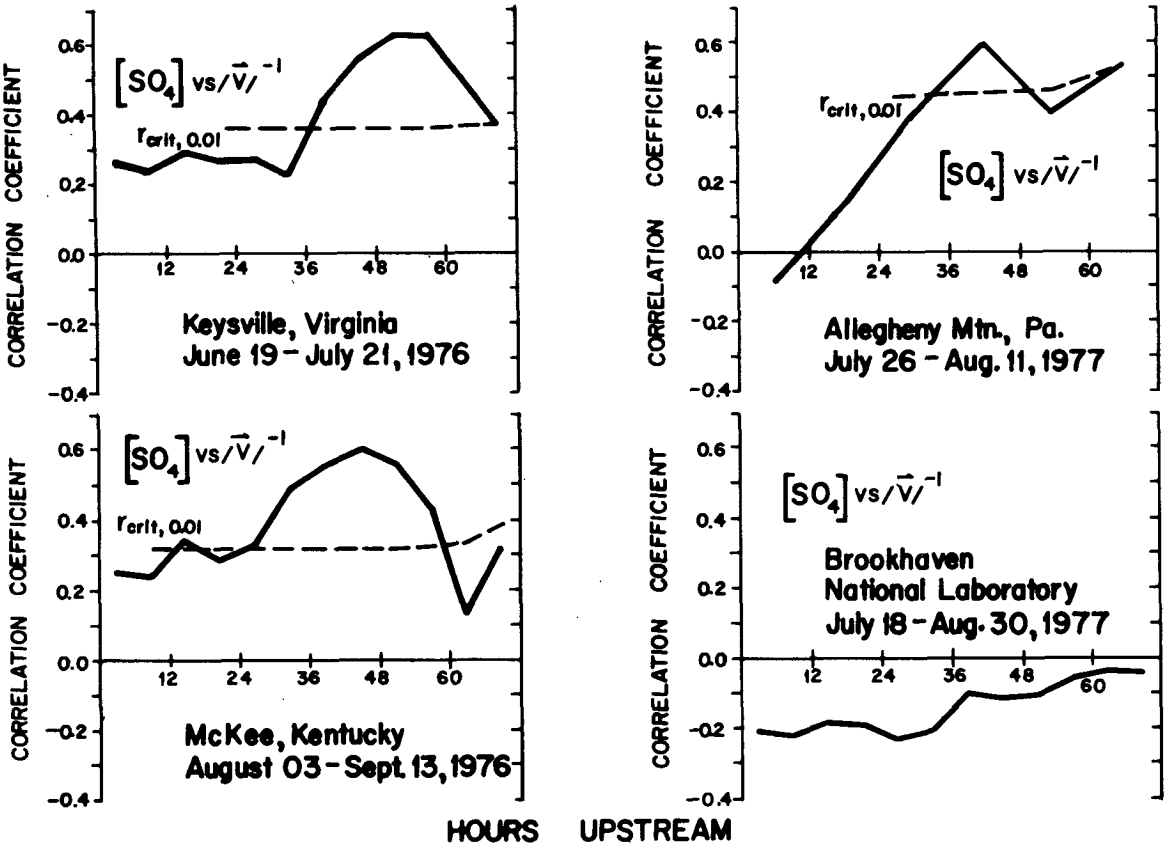

FIG. 13. Correlation coefficients as a function of hours upstream between the inverse of wind speed and resultant sulfate concentrations measured at four sites in the northeastern United States.

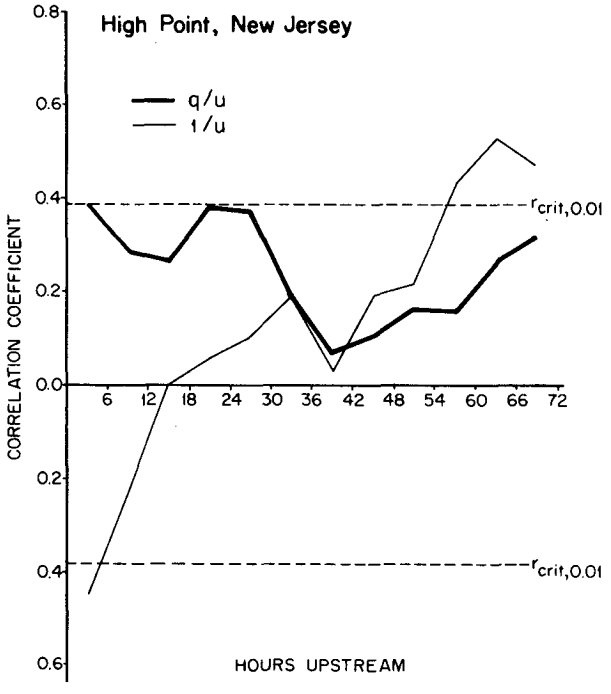

FIG. 14. The correlation coefficients between measured sulfate concentrations and the estimated upstream emissions rate q/U (kg km^{-2}), for High Point, New Jersey. Also shown is the correlation function between sulfate and $1/U$ alone.

tion; P. J. Lioy, New York University Institute of Environmental Health; G. T. Wolff, General Motors Research Laboratory; R. L. Tanner, Brookhaven National Laboratory; and W. R. Pierson, Ford Motor Company Scientific Laboratory. The author also gratefully acknowledges the support and encouragement of S. T. Rao of the New York State Department of Environment Conservation.

The author would also like to thank Mr. Dale Conventry of the U.S. Environmental Protection Agency for his initial help with the trajectory model and Mr. Thomas Whittaker, University of

TABLE 4. The total efficiency of the sulfur dioxide to sulfate conversion process as calculated from mass balance of observed sulfate to the estimated emissions burden of sulfur dioxide upstream of the sampling points.

Site	Efficiency
High Point, NJ	0.246
Allegheny, PA	0.213
Keysville, VA	0.295
McKee, KY	0.197
Brookhaven, NY	0.137
Holland, NY	0.257
Schoharie, NY	0.182
Whiteface Mt., NY	0.273

TABLE 5. The classification of sulfur dioxide to sulfate conversion efficiency as a function of resultant sulfate concentration for four sites in the northeastern United States.

Site	Concentration ($\mu g\ m^{-3}$)	ϵ	Sample size
High Point, NJ	0–10	0.091	9
	10–15	0.191	12
	15–20	0.302	7
	20–25	0.356	8
	>25	0.358	7
Allegheny Mtn.	0–5	0.055	4
	5–10	0.131	9
	10–15	0.211	9
	>15	0.320	13
Keysville, VA	0–5	0.137	18
	5–10	0.158	11
	10–20	0.397	10
	>20	0.572	12
McKee, KY	0–5	0.058	21
	5–10	0.115	19
	10–15	0.271	10
	>15	0.447	15

Wisconsin-Madison, for his help with the mapping software.

REFERENCES

Amdur, M. O., T. R. Lewis, M. P. Fitzhand and K. I. Campbell, 1972: Toxicology of atmospheric sulfur dioxide decay products. Publ. No. AP-111, Environmental Protection Agency, Research Triangle Park, NC.

Bolin, B. and C. Persson, 1975: Regional dispersion and deposition of atmospheric pollutants with particular application to sulfur pollution over western Europe. *Tellus*, **27**, 281–310.

Chung, Y. S., 1978: The distribution of atmospheric sulfates in Canada and its relationship to long-range transport of air pollutants. *Atmos. Environ.*, **12**, 1471–1480.

Coffey, P. E., P. J. Galvin, P. J. Samson, and J. Cline, 1979: Results from the 1977 special sulfate sampling network. New York State Dept. Environmental Conservation Report, Albany.

Durst, C. S., A. F. Crossley and N. E. Davis, 1959: Horizontal diffusion in the atmosphere as determined by geographic trajectories. *J. Fluid Mech.*, **6**, 401–422.

Environmental Protection Agency, 1974: Health consequences of sulfur oxides: A report from CHESS 1970–71. Environmental Protection Agency, EPA-650/1-74-004, Research Triangle Park, NC.

Galloway, J. N., E. G. Likens and E. S. Edgerton, 1976: Acid precipitation in the northeastern United States, pH and acidity. *Science*, **194**, 722–723.

Galvin, P. J., P. J. Samson, P. E. Coffey and D. Romano, 1978: Transport of sulfates to New York State. *Environ. Sci. Tech.*, **12**, 580–584.

Granat, L., 1972: On the relationship between pH and the chemical composition of atmospheric precipitation. *Tellus*, **24**, 550–560.

Hall, F. P., C. E. Duchon, L. G. Lee and R. R. Hagan, 1975: Long-range transport of air pollution: a case study, August, 1970. *Mon. Wea. Rev.*, **101**, 404–411.

Heffter, J. L., A. D. Taylor and G. J. Ferber, 1975: A regional-continental scale transport, diffusion and deposition model. NOAA Tech. Memo. ERL-ARL-50, 28 pp.

Likens, G. E., 1976: Acid precipitation. *Chem. Eng. News*, November 22, 44–99.

Lioy, P. J., G. T. Wolff, J. S. Czachor, P. E. Coffey, W. N. Stasiuk and D. Romano, 1977: Evidence of high atmospheric concentrations of sulfates detected at rural sites in the Northeast. *J. Environ. Sci. Health*, **A12**, 1–14.

McJilton, E. E., N. T. Frank and R. Charlston, 1973: Role of relative humidity in the synergistic effect of a sulfur dioxide-aerosol mixture in the lung. *Science*, **182**, 503–504.

Pierson, W. R., W. W. Brachaczek, T. J. Truex, J. W. Butler, and T. J. Korniski, 1979: Ambient sulfate measurements on Allegheny Mountain and the question of atmospheric sulfate in the northeastern United States. *Ann. N.Y. Acad. Sci.*, **338**, 145–173.

Rodhe, H., 1978: Budgets and turn-over times of atmospheric sulfur compounds. *Atmos. Environ.*, **12**, 671–680.

Samson, P. J., 1978: Ensemble trajectory analysis of summertime sulfate concentrations in New York State. *Atmos. Environ.*, **12**, 1889–1893.

——, and K. W. Ragland, 1977: Ozone and visibility reduction in the midwest: evidence of large-scale transport. *J. Appl. Meteor.*, **16**, 1101–1106.

Stasiuk, W. N., P. E. Coffey and R. F. McDermott, 1975: Relationship between suspended sulfates and ozone at a non-urban site. Paper 75-67, presented at the 68th Annual Meeting of the APCA. Boston, 15 June 1975.

Tanner, R., 1979: Sulfate, nitrate and related ionic species in airborne particulates. *Ann. N.Y. Acad. Sci.*, **338**, 39–49.

Waggoner, A. P., A. H. Vanderpol, R. J. Charlson, L. Grant, C. Tragard and S. Laisen, 1975: The sulfate light scattering ratio: an index of the role of sulfur in tropospheric optics. *Nature*, **261**, 120–122.

Whitby, K. T., 1978: The physical characteristics of sulfur aerosols. *Atmos. Environ.*, **12**, 135–160.

Wolff, G. T., P. J. Lioy, G. D. Wight, R. E. Meyers and R. T. Cederwall, 1977: An investigation of long-range transport of ozone across the midwestern and eastern United States. *Atmos. Environ.*, **11**, 797–802.